JOURNAL OF Materials CHEMISTRY

Optimization of the thermopower of the antimonide Mo_3Sb_7 by a partial Sb/Te substitution

Enkhtsetseg Dashjav, Aleksandra Szczepenowska and Holger Kleinke*

Department of Chemistry, University of Waterloo, Waterloo, Ontario, N2L 3G1, Canada. E-mail: kleinke@uwaterloo.ca

Received 16th August 2001, Accepted 5th November 2001
First published as an Advance Article on the web 3rd January 2002

The binary antimonide Mo_3Sb_7 is metallic with poor thermoelectric properties. Since band structure calculations indicated a possible change to semiconducting behavior by adding two more valence-electrons, the substitutional series $Mo_3Sb_{7-\delta}Te_\delta$ has been investigated. Te atoms can replace up to 2.3 Sb atoms in Mo_3Sb_7 without noticeable structural changes. This substitution leads to a dramatic enhancement in the thermopower, indicating that in fact semiconducting properties have been achieved with the synthesis of $Mo_3Sb_5Te_2$.

Introduction

Thermoelectric devices are usually comprised of narrow-gap p- and n-type semiconductors. The filled skutterudites have attracted wide interest because of their outstanding thermoelectric properties, which were described in 1996.[1] Many investigations into this structure family followed subsequently.[2–4] The general formula is $Ln_\delta M_4Sb_{12}$ with $0 \leqslant \delta \leqslant 1$, where Ln is a lanthanoid and M a valence-electron-rich transition element such as Fe, Co, Ni, …[5] While the parent compound, $LaFe_4Sb_{12}$, is metallic, $LaFe_3CoSb_{12}$ exhibits outstanding thermoelectric properties based on its experimentally determined figure-of-merit, ZT, which is defined as $ZT = TS^2\sigma/\kappa$. Therein, T is the actual temperature, S the Seebeck coefficient (thermopower), and σ and κ are the electrical and the thermal conductivities, respectively. The commercially used materials such as Bi_2Te_3 may exhibit ZT values around unity at the ideal operating temperature; the higher ZT, the better the thermoelectric performance.[6] In $LaFe_3CoSb_{12}$, ZT may become as high as 1.4 at 730 °C, for its good thermopower and electrical conductivity are combined with an extraordinarily low thermal conductivity. The latter stems from the high vibrations of the La atom situated in a large 'cage' of Sb atoms, a phenomenon usually referred to as *rattling*. The same phenomenon occurs in the most recently introduced telluride, $CsBi_4Te_6$, which may be considered as a filled variant of Bi_2Te_3 in a first approximation, with the Cs atoms rattling between Bi_2Te_3 layers.[7]

We are currently investigating the valence-electron-poor transition metal antimonides with the desire of creating semiconductors with three-dimensional extended Sb atom networks.[8] If such compounds exist, superior thermoelectric behavior may be expected. Our efforts resulted in the uncovery of the series $M_\delta Ti_{5-\delta}Sb_8$ (M = Zr, Hf, Nb, Mo), the band structure of which exhibits a pseudo-band gap above the Fermi level.[9] A similar situation occurs in Mo_3Sb_7,[10] which may become semiconducting by (formally) adding two valence-electrons.[11] With this contribution, we present our results of the substitutional solid solution $Mo_3Sb_{7-\delta}Te_\delta$ with respect to synthesis, phase range, electronic structure, and physical properties.

Experimental section

Syntheses

All reactions were carried out in evacuated fused silica tubes, starting from the elements (Mo: powder, 3–7 μm, 99.95%, Alfa Aesar; Sb: powder, −100 mesh, 99.5%, Alfa Aesar; Te: powder, −200 mesh, 99.8%, Sigma Aldrich). We always used 1.5 mmol Mo per reaction, and added the main group elements in the stoichiometric ratios, according to the general reaction equation:

$$3\,Mo + (7-\delta)\,Sb + \delta\,Te \rightarrow Mo_3Sb_{7-\delta}Te_\delta \quad (\text{with } 0 \leqslant \delta \leqslant 2.3)$$

The evacuated and sealed tubes were placed into a resistance furnace and heated up to the final reaction and annealing temperature of 750 °C. This reaction temperature ensures mobility of the main group elements, for it is above both the melting points of tellurium (450 °C) and antimony (630 °C), but *well below* the melting point of molybdenum (2620 °C). The formation of $Mo_3Sb_{7-\delta}Te_\delta$ is thus a solid/liquid reaction. Homogeneity was achieved by (i) applying a long reaction time of at least 10 days and (ii) grinding the samples, followed by reannealing at 750 °C for another 4–10 days. That all elemental antimony and tellurium have reacted to give the ternary molybdenum antimonide–tellurides, was indicated in each case by the absence of small silvery molten pieces of these main group elements. These were sometimes initially observed after a few reaction days, hinting towards incomplete reactions.

Analyses

All samples were investigated by X-ray powder diffraction to check for purity (Bruker D500, Cu Kα radiation). EDS investigations (LEO 1530, with integrated EDAX Pegasus 1200) revealed that no impurities were present. A clear quantification of the Sb and Te concentrations was impossible due to severe overlap of all their peaks (*e.g.* the Lα line energies are 3.604 and 3.769 keV, respectively). Homogeneous samples were obtained for all reactions aiming at $Mo_3Sb_{7-\delta}Te_\delta$ with $0 \leqslant \delta \leqslant 2.3$; higher Te contents led to the formation of α-$MoTe_2$ (MoS_2-type).[12] Rietveld refinements (FULLPROF) showed only minor changes in the crystal structures with increasing δ (see, for example, Fig. 1). The lattice constants remain the same within the standard deviations upon Te incorporation, *i.e.* the *a* axis was refined to 956.1(1) pm for Mo_3Sb_7 and 956.3(1) pm for $Mo_3Sb_5Te_2$. Because of the comparable scattering factors of Sb and Te, we carried out all refinements using the Mo_3Sb_7 structure model.

Since the only published data on the refinement of the Mo_3Sb_7 structure were obtained from Weissenberg photographs with a final $R(F) = 0.094$,[13] we carried out a new refinement on a cubic-shaped single crystal using the Smart

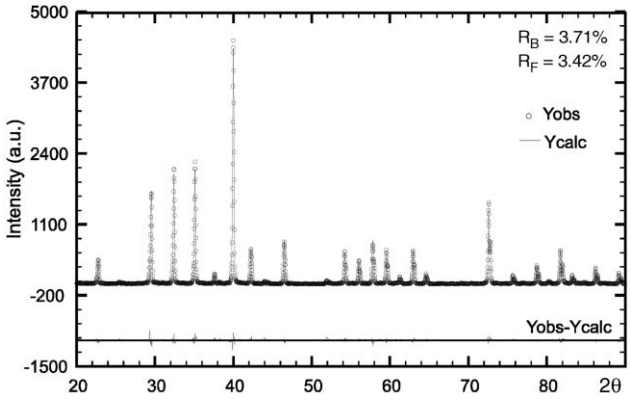

Fig. 1 Rietveld refinement of $Mo_3Sb_5Te_2$ using Mo_3Sb_7 as the structure model.

Apex CCD (Bruker).[14] A summary of all crystallographic data is given in Table 1, which will be discussed below.

Computations

Self-consistent LMTO calculations (LMTO = linear muffin tin orbitals)[15–17] were carried out on Mo_3Sb_7 and on different models simulating $Mo_3Sb_5Te_2$. Therein, the density functional theory was utilized with the local density approximation (LDA). The integration in k space was performed by an improved tetrahedron method[18] on a grid of 16 × 16 × 16 k points of the first Brillouin zone (*i.e.* 145 irreducible k points from 4096).

Physical property measurements

The Seebeck coefficients were determined on cold-pressed bars of the dimensions 5 × 1 × 1 mm, using the commercial device from MMR Technologies with constantan as standard. The measurements were carried out in dynamic vacuum between 300 and 600 K. We also measured the resistances of these samples at 300 K using a standard ohmmeter.

Results and discussion

Materials properties

All samples were prepared in the form of black, microcrystalline powder. The small crystals are usually of cubic morphology. Under exclusion of air, these materials decompose peritectoidally slightly below 800 °C into elemental Mo, Sb and the telluride α-$MoTe_2$.

Crystal structure

Mo_3Sb_7 is reported to crystallize in the Ir_3Ge_7-type, which comprises a cubic body-centered unit cell, space group $Im\bar{3}m$. A projection onto the a,b plane is presented in Fig. 2. The structure contains a three-dimensional Sb atom network, which includes the Mo atoms in square antiprismatic voids. The shortest distances are the eight Mo−Sb bonds per Mo atom, namely 4 × 279 and 4 × 281 pm, according to our new single crystal data. These are slightly longer than the sum of the single bond radii of 268 pm (after Pauling:[19] r_{Mo} = 129; r_{Sb} = 139 pm). Since Mo_3Sb_7 is the only molybdenum antimonide known to date, its Mo–Sb bonds may be compared best to the shortest found in $MoSb_2Se$ (282 to 284 pm).[20]

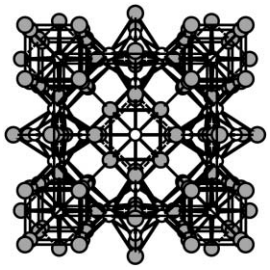

Fig. 2 Projection of the crystal structure of Mo_3Sb_7 along [001]. White circles, Mo; gray, Sb.

In addition to the heteronuclear Mo–Sb bonds, homonuclear interactions of both kinds, *i.e.* Mo–Mo and Sb–Sb, are present in Mo_3Sb_7. Two $MoSb_8$ antiprisms are condensed by sharing a square face, which occurs with the formation of a Mo pair with a Mo–Mo distance of 300 pm (left part of Fig. 3). The Sb(1)–Sb(1) contacts in this shared face (dashed lines in Fig. 3) are 338 pm, which is significantly longer than the distances between the Sb(2) atoms in the top and bottom faces of the antiprism pair (310 pm, solid lines). The antiprisms build chains running parallel to each of the crystallographic axes (which are equivalent in the cubic crystal system) by forming intermediate Sb–Sb bonds between each pair of $MoSb_8$ antiprisms. This results in the formation of empty $Sb(2)_8$ cubes alternating with pairs of $MoSb_8$ antiprisms along each axis. Parallel running chains are interconnected *via* the shortest Sb–Sb bond of this structure (291 pm) between the $Sb(2)_8$ cubes. The right part of Fig. 3 illustrates the plane perpendicular to the chain direction of the left part. Since each face of the $Sb(2)_8$ cube is also a part of a $MoSb_8$ square antiprism, each cube is a crossing point of three perpendicular running chains of antiprisms.

The Mo–Mo bonds in $MoSb_2Se$ and in β-$MoTe_2$[21] are between 281 and 290 pm, where each Mo^{+4} atom takes part in two Mo–Mo bonds described best as single bonds. Thus, the much longer interaction in Mo_3Sb_7 (300 pm) is most likely weakly bonding, if at all. Sb–Sb single bonds are in the range of 280 to 290 pm, *e.g.* 283 and 285 in the Zintl compound KSb,[22] comparable with the short Sb(2)–Sb(2) bond of 291 pm in

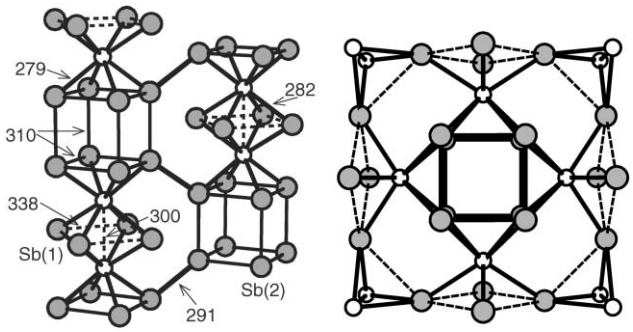

Fig. 3 Left: two parallel chains of $MoSb_8$ square antiprisms; right: the $MoSb_8$ antiprisms centered around the empty $Sb(2)_8$ cube.

Table 1 Crystallographic data[a]

Formula	a/pm	x(Mo)	x(Sb(2))	Method	$R(F)$
Mo_3Sb_7[b]	957.13(8)	0.3425(13)	0.1624(4)	Weissenberg	0.094
Mo_3Sb_7[c]	955.9(3)	0.3432(2)	0.16220(8)	CCD	0.033
Mo_3Sb_7[c]	956.1(1)	0.3451(8)	0.1633(3)	D500	0.055
$Mo_3Sb_5Te_2$[c]	956.3(1)	0.3407(5)	0.1634(2)	D500	0.037

[a]Space group $Im\bar{3}m$, Mo on x, 0, 0; Sb(1) on 1/4, 0, 1/2; Sb(2) on x, x, x. [b]Data taken from ref. 13. [c]This work.

Mo_3Sb_7, whereas bonds of 310 pm [the longer Sb(2)–Sb(2) distance] are often described as half bonds, *i.e.* having one electron per bond.[23–25] On the other hand, the long Sb(1)–Sb(1) contact (338 pm) in Mo_3Sb_7 is most likely only of weak bonding character, as comparisons with elemental antimony (a weak bond of 335 pm) or other transition metal antimonides[26–28] reveal.

To summarize, the crystal structure of Mo_3Sb_7 comprises pairs of $MoSb_8$ square antiprisms with one weakly bonding Mo–Mo interaction per pair of antiprisms, weak Sb(1)–Sb(1) bonding in the shared Sb_4 square, half Sb(2)–Sb(2) bonds forming the edges of an empty Sb_8 cube and full Sb(2)–Sb(2) bonds connecting neighboring cubes. Intercalating a cation A into this cube would lead to A–Sb(2) distances of 269 pm and A–Mo distances of 328 pm.

According to the results of the Rietveld refinements (Table 1), only minor changes occur when replacing Sb atoms in part with Te atoms. The most significant change is in the *x* parameter of the Mo atom, which comes along with an increase of the Mo–Mo distance from 300 to 305 pm. This indicates a weakened Mo–Mo bond by filling antibonding states with the additional valence-electron stemming from the Sb/Te exchange.

Electronic structure

The band structure of Mo_3Sb_7 is shown in the left part of Fig. 4. Several bands cross the Fermi level, E_F, along all symmetry lines selected (chosen according to Bradley and Cracknell[29]), resulting in Mo_3Sb_7 being a material with three-dimensional metallic properties. The bands with mostly Sb p character are emphasized *via* the *fat band* representation.[30] With respect to thermoelectric properties, it is important to note the band gap that is located two valence-electrons per formula unit above E_F, as well as the presence of numerous flat bands in the area around E_F, which indicate high effective band masses that may occur with high thermopower.[31]

The densities of states of Mo_3Sb_7 reveal that both atom kinds, Mo and Sb, contribute significantly to the region around E_F (right part of Fig. 4). A band gap of *ca.* 0.9 eV occurs above the Fermi level, E_F. A smaller gap, namely of the size of a few tenths of an eV (*i.e.* 6–10 k_BT where k_B = Boltzman constant, T = temperature) is recommended for high thermopower materials.[32,33] The region around E_F is dominated by Mo d states, whereas most of the Sb contributions are located well below and partly above E_F.

The Mo–Sb, Mo–Mo, and Sb–Sb COHP (crystal orbital Hamilton population)[34] curves, cumulated over all of the participating interactions in the first Brillouin zone, are revealed in Fig. 5. It is evident that the heteronuclear Mo–Sb interactions are dominating; however, both the Mo–Mo and Sb–Sb interactions contribute to the stability of Mo_3Sb_7 as well. While only bonding Mo–Sb states are filled, antibonding states are found below the Fermi level for all homonuclear interactions.

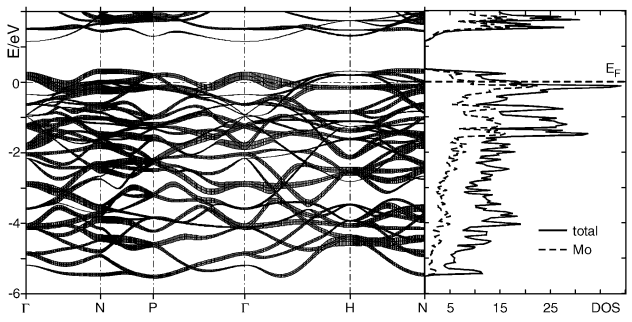

Fig. 4 Band structure [left, emphasizing the Sb(1) contributions], and densities of states (DOS) of Mo_3Sb_7 (right).

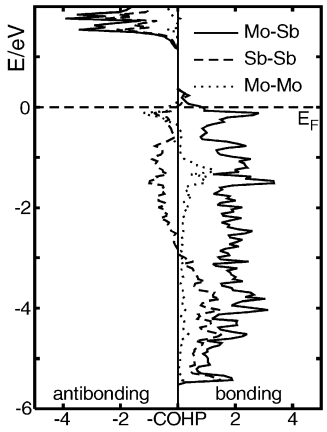

Fig. 5 Cumulated COHP curves of Mo_3Sb_7.

However, integrating over all filled states gives net bonding character in all cases. These integrations can be quantified in the ICOHP values, which are measures for relative bond strengths. The ICOHP values are −2.03 and −1.62 eV per bond for the two different Mo–Sb bonds, −1.01 for the Mo–Mo bond, and −0.79, −0.40, and −0.10 for the three different Sb–Sb bonds. It must be noted that negative ICOHPs indicate bonding interactions. Very few ICOHP values have been published thus far, likely the first calculated values were for the strongest bonds in some 3d elements. These are −1.53 eV per bond in elemental iron, −1.22 in cobalt and −1.00 in nickel.[35]

We calculated the ICOHPs of the various bonds in elemental molybdenum and antimony as well as in KSb for comparison. The bond lengths in molybdenum (cubic body-centered packing) are 273 and 315 pm with ICOHPs of −2.12 and −0.77 eV per bond, respectively. We thus state that the Mo–Mo bond in Mo_3Sb_7 (300 pm, −1.01 eV) is stronger than the longer bond in the element. The single Sb–Sb bonds in KSb (283 and 285 pm) have ICOHPs of −2.29 and −1.87, respectively, whereas the two bonds in elemental antimony (291 and 335 pm) have ICOHPs of −1.63 and −0.26. It can therefore be concluded that at least the two shorter Sb–Sb distances in Mo_3Sb_7 have bonding character with ICOHPs of −0.79 and −0.40 eV per bond.

Raising the valence-electron concentration and thereby raising the Fermi level into the band gap would occur with an increase in overall Mo–Sb and Sb–Sb bonding because of an increase in filled bonding states, but a decrease in Mo–Mo bonding due to antibonding Mo–Mo states becoming filled. This is in agreement with the observed elongation of the Mo–Mo bond upon increasing the valence-electron number by the partial substitution of Sb with Te atoms.

Reasonable experimental possibilities to raise the valence-electron concentration include a partial Sb/Te exchange, as successfully done during this work, or intercalations of electron donors such as electropositive metal atoms (like Na, K, Mg, Ca, Ti,… Cu) – we are currently exploring the latter approach as well. This can be a very effective method of also lowering the lattice contributions to the thermal conductivity by producing the *rattling* effect.

The advantage of the Sb/Te substitution lies in the similarity of Sb and Te atoms; one can thus assume that the band dispersions will not change too much. To investigate this, we calculated the band structures of different structure models of $Mo_3Sb_5Te_2$. Owing to the higher electronegativity of Te, compared to Sb, we propose that Te atoms prefer the site with weaker Q–Q interactions (Q = Sb, Te), namely the one in the large Q_4 square [originally $Sb(1)_4$ square], and that Te–Te contacts are minimized. Two of the three Sb(1) atoms per formula unit $Mo_3Sb(1)_3Sb(2)_4$ have to be replaced by Te atoms.

However, since we could not experimentally distinguish between the Sb and Te sites, it is thus unclear whether or not the Te atoms are located in an ordered way throughout the unit cell, which we have to assume for the band structure calculations. Two different models were considered. In model **I**, the original unit cell was retained, but the 3-fold rotational axis was destroyed by introducing the Te atoms, leading to the space group *I*4/*mmm* in the tetragonal crystal system. The Sb/Te coloring is shown in the left part of Fig. 6, a projection along the tetragonal *c* axis. No Sb(1)–Sb(1) contacts remain, the shortest Te–Te contacts are 338 pm. In the second model (model **II**, right part of Fig. 6), the unit cell was enlarged according to the transformation matrix (1 0 $\bar{1}$, 0 1 0, 1 0 1), while reducing the symmetry to the orthorhombic space group *F*2*mm*. The main difference between models **I** and **II** is the occurrence of Sb(1) pairs in model **II** (distance 338 pm).

First, we consider model **I**. Its band structure and densities of states are illustrated in Fig. 7. Since tellurium is the most electronegative element in $Mo_3Sb_5Te_2$, its valence-orbitals are found well below the Fermi level, E_F. Two major differences of the band structure of model **I**, compared to the Mo_3Sb_7 band structure, are: (i) the Fermi level falls right into the band gap, as anticipated; and (ii) the size of the band gap decreases from 0.9 to 0.5 eV. Both differences mark an improvement in the thermopower.

The decrease of the band gap results from raising the highest occupied bands at the P point [mainly Sb(1) p character] and at the H point (Mo d band), while the band dispersions above E_F remain principally unchanged. Minor changes, of course, stem from the lower symmetry occurring with smaller degeneracies, *e.g.* at the Γ point.

The same is true for the band structure of model **II** (Fig. 8), which is also a small-gap semiconductor. A major difference between the models **I** and **II** is the occurrence of a direct gap in **II**, whereas **I** exhibits an indirect band gap. Since these are just

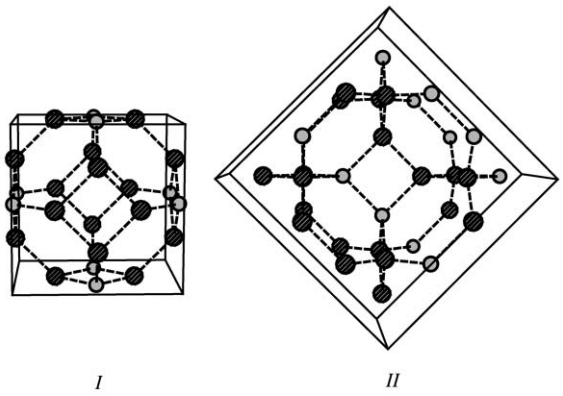

Fig. 6 Sb(1)–Te fragments of the structure models **I** (left) and **II** (right). Hatched circles, Te atoms.

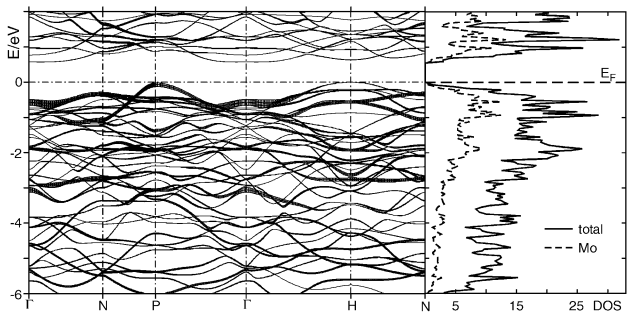

Fig. 7 Band structure [left, emphasizing the Sb(1) contributions] and DOS (right) of structure model **I** ($Mo_3Sb_5Te_2$ in *I*4/*mmm*).

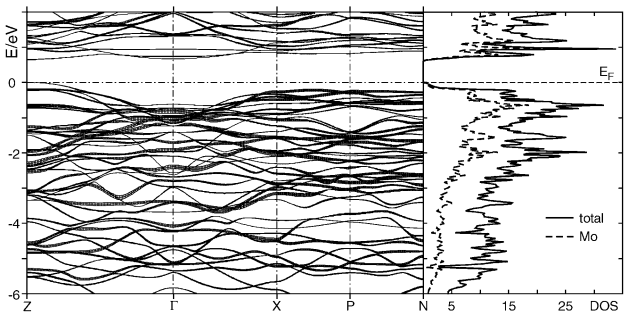

Fig. 8 Band structure [left, emphasizing the Sb(1) contributions] and DOS (right) of structure model **II** ($Mo_3Sb_5Te_2$ in *F*2*mm*).

structure models, these details shall not be overemphasized at this moment.

Physical properties

According to our experiments, up to 2.3 Sb atoms of Mo_3Sb_7 may be replaced by Te atoms. We measured the thermopower (Seebeck coefficients *S*) of the series $Mo_3Sb_{7-\delta}Te_\delta$ with $\delta = 0.0$, 1.8, 1.9, 2.0, 2.1, 2.2, and 2.3 between 300 and 600 K (Fig. 9). In each case, *S* increases (more or less smoothly) with increasing temperature. Mo_3Sb_7 exhibits the smallest *S* over the whole temperature region measured, with *S* ranging between $+26\ \mu V\ K^{-1}$ at 300 K and $+53\ \mu V\ K^{-1}$ at 600 K. These values are slightly higher than in most other metallic compounds, which usually have thermopower values between −20 and $+20\ \mu V\ K^{-1}$. Examples for metals with comparably high thermopowers include chromium ($S = +22$), europium (+25), ytterbium (+30), scandium (−19) and cobalt ($-31\ \mu V\ K^{-1}$ at 300 K).[6]

The thermopower *S* increases in the series $Mo_3Sb_{7-\delta}Te_\delta$ with increasing Te content (thus increasing valence-electron concentrations), until the maximum is reached at $\delta = 2.2$ with $S = +93\ \mu V\ K^{-1}$ at 300 K and $+190\ \mu V\ K^{-1}$ at 600 K. These values are comparable to the thermopower of $LaFe_3CoSb_{12}$, which is about +100 at 300 K and below $+200\ \mu V\ K^{-1}$ at 600 K.[1] Higher Te contents in $Mo_3Sb_{7-\delta}Te_\delta$ (*i.e.* $\delta > 2.2$) occur with lower Seebeck coefficients (Fig. 10).

Theoretically, even higher Te contents should lead to a negative thermopower, since eventually the electrons should dominate as the charge carriers. This point could not be reached experimentally, for increasing the Te content led to the formation of $MoTe_2$ in addition to $Mo_3Sb_{7-\delta}Te_\delta$. Hypothetically, the crossover between positive and negative thermopower would occur at $\delta = 2$. Since this is not observed below $\delta = 2.3$, it is concluded that $Mo_3Sb_5Te_2$ is a semiconductor with intrinsic p-type character. The same is true for $LaFe_{4-\delta}Co_\delta Sb_{12}$ (p-type at $\delta = 1$)[1] and $Bi_{2+\delta}Te_{3-\delta}$ (n-type at $\delta = 0$).[36] In the latter case, the transition between p- and n-type takes place at 63 at.% Te (hypothetical value: 66.7% Te). $Nb_3Sb_2Te_5$,[37] which is isostructural and

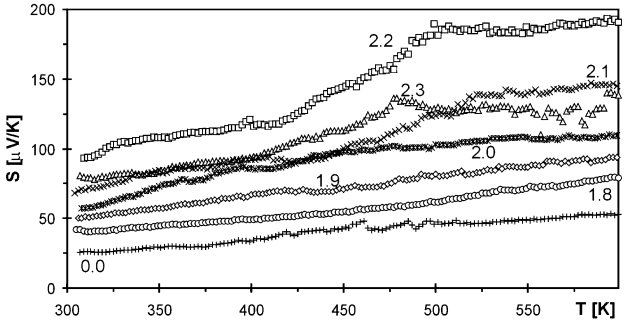

Fig. 9 Temperature dependence of the Seebeck coefficients of $Mo_3Sb_{7-\delta}Te_\delta$. δ is given close to the respective data.

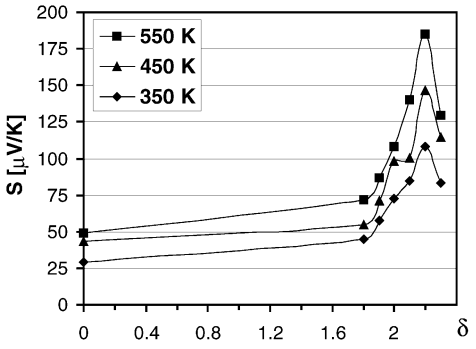

Fig. 10 Seebeck coefficients at 350, 450 and 550 K of $Mo_3Sb_{7-\delta}Te_\delta$ *versus* δ.

isoelectronic with $Mo_3Sb_5Te_2$, is also an intrinsic p-type semiconductor. According to our measurements, its room temperature thermopower is as low as $+18\ \mu V\ K^{-1}$. However, we are currently trying to optimize this value by changing the Sb/Te ratio in the niobium compound as well.

The absolute electrical conductivity σ decreases by a factor of 5 by going from Mo_3Sb_7 to $Mo_3Sb_{4.8}Te_{2.2}$. Combined with the increase of the Seebeck coefficient of a factor of almost four (*i.e.* from 26 to 94 $\mu V\ K^{-1}$, corresponding to a factor of 3.6), the power factor alone, defined by $S^2\sigma$, increases by $3.6^2/5 = 2.6$. In addition to this increase, the thermal conductivity, composed of the sum of the lattice and the electronic contributions, $\kappa_{Ph} + \kappa_{el}$, will decrease because the ratio of σ/κ_{el} is constant at any given temperature (Wiedemann–Franz law).[6] Based on the thus improved figure-of-merit $ZT = TS^2\sigma/(\kappa_{Ph} + \kappa_{el})$, the thermoelectric properties in total are superior in the case of the ternary antimonide–telluride because of the higher power factor $S^2\sigma$ and the lower thermal conductivity, κ_{el}, compared to Mo_3Sb_7.

Conclusion

Mo_3Sb_7 was rendered semiconducting by a partial Sb/Te replacement. $Mo_3Sb_{7-\delta}Te_\delta$ exists with $0 \leqslant \delta \leqslant 2.3$. The thermopower reaches a maximum at $\delta = 2.2$, which is comparable to the values found in the ideal filled skutterudites (*e.g. ca.* $100\ \mu V\ K^{-1}$ at room temperature). Since increasing temperature occurs with increasing thermopower, the material might be more interesting for high temperature applications. The two other key properties of the thermoelectric energy conversion, however, remain to be determined in detail for more accurate results.

Acknowledgements

Financial support from the Canadian Foundation for Innovation, the Ontario Innovation Trust, the Materials Manufacturing Ontario, the Province of Ontario, and the National Science and Engineering Research Council of Canada is appreciated.

References

1 B. C. Sales, D. Mandrus and R. K. Williams, *Science*, 1996, **272**, 1325.
2 G. S. Nolas, D. T. Morelli and T. M. Tritt, *Annu. Rev. Mater. Sci.*, 1999, **29**, 89.
3 G. S. Nolas, M. Kaeser, R. T. Littleton IV and T. M. Tritt, *Appl. Phys. Lett.*, 2000, **77**, 1855.
4 N. R. Dilley, E. D. Bauer, M. B. Maple, S. Dordevic, D. N. Basov, F. Freibert, T. W. Darling, A. Migliori, B. C. Chakoumakos and B. C. Sales, *Phys. Rev. B*, 2000, **61**, 4608.
5 W. Jeitschko and D. Braun, *Acta Crystallogr., Sect. B*, 1977, **33**, 7.
6 D. M. Rowe and C. M. Bahandri, *Modern Thermoelectrics*, Holt Saunders, London, 1983.
7 D. Y. Chung, T. Hogan, P. Brazis, M. Rocci-Lane, C. Kannewurf, M. Bastea, C. Uher and M. G. Kanatzidis, *Science*, 2000, **287**, 1024.
8 H. Kleinke, *Chem. Soc. Rev.*, 2000, **29**, 411.
9 H. Kleinke, *Inorg. Chem.*, 2001, **40**, 95.
10 A. Brown, *Nature*, 1965, **206**, 502.
11 U. Häussermann, M. Elding-Pontén, C. Svensson and S. Lidin, *Chem. Eur. J.*, 1998, **4**, 1007.
12 D. Puotinen and R. E. Newnham, *Acta Crystallogr.*, 1961, **14**, 691.
13 P. Jensen and A. Kjekshus, *Acta Chem. Scand.*, 1966, **20**, 417.
14 *Crystal data*: Mo_3Sb_7, $M = 1140.07\ g\ mol^{-1}$; space group $Im\bar{3}m$; lattice parameter $a = 955.9(3)$ Å; $Z = 4$; $\mu = 25.3\ mm^{-1}$; 198 independent reflections; $R(F) = 0.033$, $R_w(F^2) = 0.047$ for 130 observed reflections [$I > 2\sigma(I)$]. Atomic positions (atom: x, y, z, U_{eq}/pm^2): Mo: 0.3432(2), 0, 0, 81(3); Sb(1): 1/4, 0, 1/2, 99(3); Sb(2): 0.16220(8), x, x, 102(3).
15 U. van Barth and L. Hedin, *J. Phys. C*, 1971, **4**, 2064.
16 O. K. Andersen, *Phys. Rev. B*, 1975, **12**, 3060.
17 H. L. Skriver, *The LMTO Method*, Springer, Berlin, 1984.
18 P. E. Blöchl, O. Jepsen and O. K. Andersen, *Phys. Rev. B*, 1994, **49**, 16 223.
19 L. Pauling, *The Nature of the Chemical Bond*, Cornell University Press, Ithaca, NY, 3rd edn., 1948.
20 H. Kleinke, *Chem. Commun.*, 2000, 1941.
21 B. E. Brown, *Acta Crystallogr.*, 1966, **20**, 268.
22 W. Hönle and H.-G. von Schnering, *Z. Kristallogr.*, 1981, **155**, 307.
23 M. J. Ferguson, R. J. Hushagen and A. Mar, *J. Alloys Compd.*, 1997, **249**, 191.
24 H. Kleinke, *Eur. J. Inorg. Chem.*, 1998, 1369.
25 G. A. Papoian and R. Hoffmann, *Angew. Chem., Int. Ed.*, 2000, **39**, 2408.
26 H. Kleinke, *Inorg. Chem.*, 1999, **38**, 2931.
27 H. Kleinke, *J. Mater. Chem.*, 1999, **9**, 2703.
28 H. Kleinke, *J. Am. Chem. Soc.*, 2000, **122**, 853.
29 C. J. Bradley and A. P. Cracknell, *The Mathematical Theory of Symmetry in Solids*, Clarendon Press, Oxford, 1972.
30 O. Jepsen and O. K. Andersen, *Z. Phys.*, 1995, **97**, 25.
31 F. J. DiSalvo, *Science*, 1999, **285**, 703.
32 J. O. Sofo and G. D. Mahan, *Phys. Rev. B*, 1994, **49**, 4565.
33 G. D. Mahan and J. O. Sofo, *Proc. Natl. Acad. Sci. USA*, 1996, **93**, 7436.
34 R. Dronskowski and P. Blöchl, *J. Phys. Chem.*, 1993, **97**, 8617.
35 G. A. Landrum and R. Dronskowski, *Angew. Chem., Int. Ed.*, 2000, **39**, 1560.
36 J. P. Fleurial, J. Gailliard, R. Triboulet, H. Scherrer and S. Scherrer, *J. Phys. Chem. Solids*, 1988, **49**, 1237.
37 P. Jensen and A. Kjekshus, *J. Less-Common Met.*, 1967, **13**, 357.